Roberts, Hannah ; Price, Roy ; Brombach, Christoph-Cornelius ; Pichler, Thomas

Mercury in the hydrothermal fluids and gases in Paleochori Bay, Milos, Greece

Journal Article	as:	peer-reviewed accepted version (Postprint)
DOI of this document*(secondary publication):		https://doi.org/10.26092/elib/3129
Publication date of this document:		02/12/2024

* for better findability or for reliable citation

Recommended Citation (primary publication/Version of Record) incl. DOI:

Roberts, Hannah ; Price, Roy ; Brombach, Christoph-Cornelius ; Pichler, Thomas. 2021. Poor drainage-induced waterlogging in Saharan groundwater-irrigated lands: Integration of geospatial, geophysical, and hydrogeological techniques. Marine Chemistry, vol. 233. © Elsevier.
DOI: 10.1016/j.marchem.2021.103984.

Mercury in the hydrothermal fluids and gases in Paleochori Bay, Milos, Greece

Hannah Roberts [a,*], Roy Price [b], Christoph-Cornelius Brombach [a], Thomas Pichler [a]

[a] Universität Bremen, Fachbereich Geowissenschaften, Geochemistry and Hydrogeology, Klagenfurter Str. 2-4, 28359, Bremen, Germany
[b] Stony Brook University, School of Marine and Atmospheric Sciences, Stony Brook, New York, USA

A B S T R A C T

Seafloor hydrothermal activity may constitute a considerable mercury (Hg) source to the oceans, but the flux from marine shallow-water hydrothermal systems (MSWHS) remains poorly constrained to date. To study the presence of Hg in MSWHS in Paleochori Bay (Milos Island, Greece), sea surface, bottom, pore fluid and hydrothermal gas samples were collected in June of 2017, October of 2018 and July of 2020, and analyzed for Cl, Br, SO_4, As, Ca, Fe, K, Mg, Mn, Na, Si, Sr, H_2S, unfiltered total Hg (THg), and filtered Hg (Hg_{diss}). Specific sites were selected for the analysis of volatile elemental Hg (Hg^o), dimethylmercury (DMHg), monomethylmercury (MMHg), and Hg in the gas phase (Hg_{gas}). Concentrations of THg observed in samples collected from the sea surface were elevated compared to surface samples taken outside Paleochori Bay. The highest surface water concentrations (~10 to 15 pM) were measured in samples collected directly above shallow-water hydrothermal discharge areas. Pore fluids outside Paleochori Bay were significantly lower in THg (0.8 to 8.6 pM) than those taken inside (17.4 to 1511 pM). Porewaters collected from areas with visible gaseous or fluid emission were highly variable but generally elevated in THg concentrations (185 to 5066 pM). Concentrations within gases ranged from 0.7 to 2791 nmol/m^3. The vast majority of samples with highly elevated THg (> 100 pM) had low Na/K ratios (< 15), indicative of rapidly rising fluid. Concentrations of Hg^0, DMHg, and MMHg were below detection limits in all samples.

Bottom substrate type (e.g., rocky vs. sediment covered) likely affected infiltration rates of oxygenated seawater below the sediment-water interface, thereby affecting Hg speciation and removal by precipitation. Flux rates from porewaters compared to those with gaseous emission were high (12.56 to 1088 mol THg/year and 0.37 to 1.85 mol THg/year). Sites with slow gaseous emission rates are hypothesized to have extended subsurface reaction times, resulting in lower Hg concentrations emitted to bottom waters. However, increasing rates of gas emission did not necessarily indicate higher Hg concentrations. The scavenging of Hg in the sediments and advective flux out of Paleochori Bay likely prevent significant accumulations of THg in the water column of Paleochori Bay. The total atmospheric flux from Paleochori Bay using average flux calculations over the entire surface area would contribute 6 mmol Hg/year to the atmosphere.

We hypothesize that Hg concentrations within the pore fluids of Paleochori Bay reflect a balance between mixing and precipitation in the subsurface. A three-component mixing system of vapor, brine and seawater determines THg concentrations; however, precipitation due to sulfur cycling, changes in redox conditions and temperature, all play a crucial role in removing Hg from emitted fluids and gases.

1. Introduction

Mercury (Hg) is a post-transition metal with unique physicochemical properties and a rather distinct global biogeochemical cycle. Contrary to other trace metals, it is highly volatile and has a low chemical reactivity in its gaseous elemental form (Hg^0). Consequently, it has an atmospheric residence time of close to one year and is thus widely dispersed worldwide (Schroeder and Munthe, 1998). In the marine environment, Hg is a scavenged trace element and can be present in two oxidation states: elemental Hg^0 and ionic Hg^{2+}. Elemental Hg is generally present as a dissolved gas but can also be bound to particulates (Wang et al., 2015). Ionic Hg is mainly associated with sulfur minerals and methylated

* Corresponding author.
E-mail address: roberts@uni-bremen.de (H. Roberts).

organic species monomethylmercury (MMHg) and dimethylmercury (DMHg). Biotic and abiotic processes control the speciation and complexation of Hg, which determine Hg availability for methylation and toxicity (Fitzgerald et al., 2007; Mason, 2001). Dissolved species (Hg_{diss}) include Hg bound to colloids (< 0.45 μm) and unbound Hg^{2+} and Hg^0, and methylated species. Both Hg^0 and DMHg are volatile. Concentrations of bound Hg^0 can be significant and prevent the escape of Hg^0 to the atmosphere; however, their stability is unknown. Total Hg (THg) concentrations in unpolluted waters for the Mediterranean Sea were reported to be in the low pM range (Cossa et al., 1997; Horvat et al., 2003) with a varying temporal and spatial distribution in the water column (Fitzgerald et al., 2007; Gworek et al., 2016).

Methylmercury (MeHg) is of particular concern as it is a bioaccumulating toxin causing adverse health effects for organisms at higher trophic levels (Frederick and Jayasena, 2010) and their human consumers (Fitzgerald and Clarkson, 1991). Anthropogenic Hg emissions, mainly due to coal combustion and artisanal and small-scale gold mining, have exceeded natural emissions since the onset of the industrial revolution (Sun et al., 2014; UNEP, 2013). Those emissions increased the marine Hg inventory (Lamborg et al., 2014), amplified MeHg production and bioaccumulation, and increased human exposure. Therefore, the production of methylated species by biotic and abiotic mechanisms is of interest, along with inorganic Hg sources.

Fluid and gas emissions from subaerial, deep-sea and marine shallow-water hydrothermal systems (MSWHS) are enriched in Hg, but conclusions regarding the importance of MSWHS as part of the global Hg cycle remain uncertain. Studies regarding Hg concentrations in MSWHS are limited and data only exists for the sites in Bahia Concepcion and Panarea Island. (e.g., Bagnato et al., 2017; Leal-Acosta et al., 2010). Nevertheless, some view hydrothermal venting to be the single most important primary natural Hg source to the global Hg cycle (Sonke et al., 2013). Regardless, current global Hg cycling models have either excluded or discounted MSWHS due to limited data or by extrapolating reactions observed for deep-sea systems. These models report atmospheric flux as the primary transport mechanism to the ocean (Lamborg et al., 2002; Mason and Sheu, 2002).

MSWHS are defined as occurring at seawater depths less than ~200 m and are chiefly associated with island arc volcanoes, intraplate volcanoes, and mid-ocean ridges (Price and Giovannelli, 2017). Most sites of hydrothermal activity are characterized by the emissions of gases and fluids with elevated heavy metal concentrations, high temperatures, and low pH (e.g., McCarthy et al., 2005; Pichler et al., 2019; Pichler et al., 1999b; Price and Giovannelli, 2017; Valsami-Jones et al., 2005). Hydrothermal fluids often have elevated concentrations of THg as a result of water-rock interactions and magmatic degassing (e.g., Taran et al., 1995). While Hg is known to travel in the vapor phase, mixing with other fluids such as brines and seawater, combined with a decrease in pressure and temperature, leads to the formation of Hg^{2+} and thus Hg removal from the vapor phase (Christenson and Mroczek, 2003). Therefore, Hg is emitted as both a liquid and a gas in shallow water systems.

Here, we present the first estimate of Hg flux and Hg concentrations in gases and fluids for the marine shallow-water hydrothermal system in Paleochori Bay, Milos, Greece.

2. Materials and methods

2.1. Geological setting

Paleochori Bay is located in the southeast of Milos, which is part of the Southern Aegean Volcanic Arc (Fig. 1). The island consists primarily of rhyolitic to andesitic volcanic rock atop a greenschist metamorphic

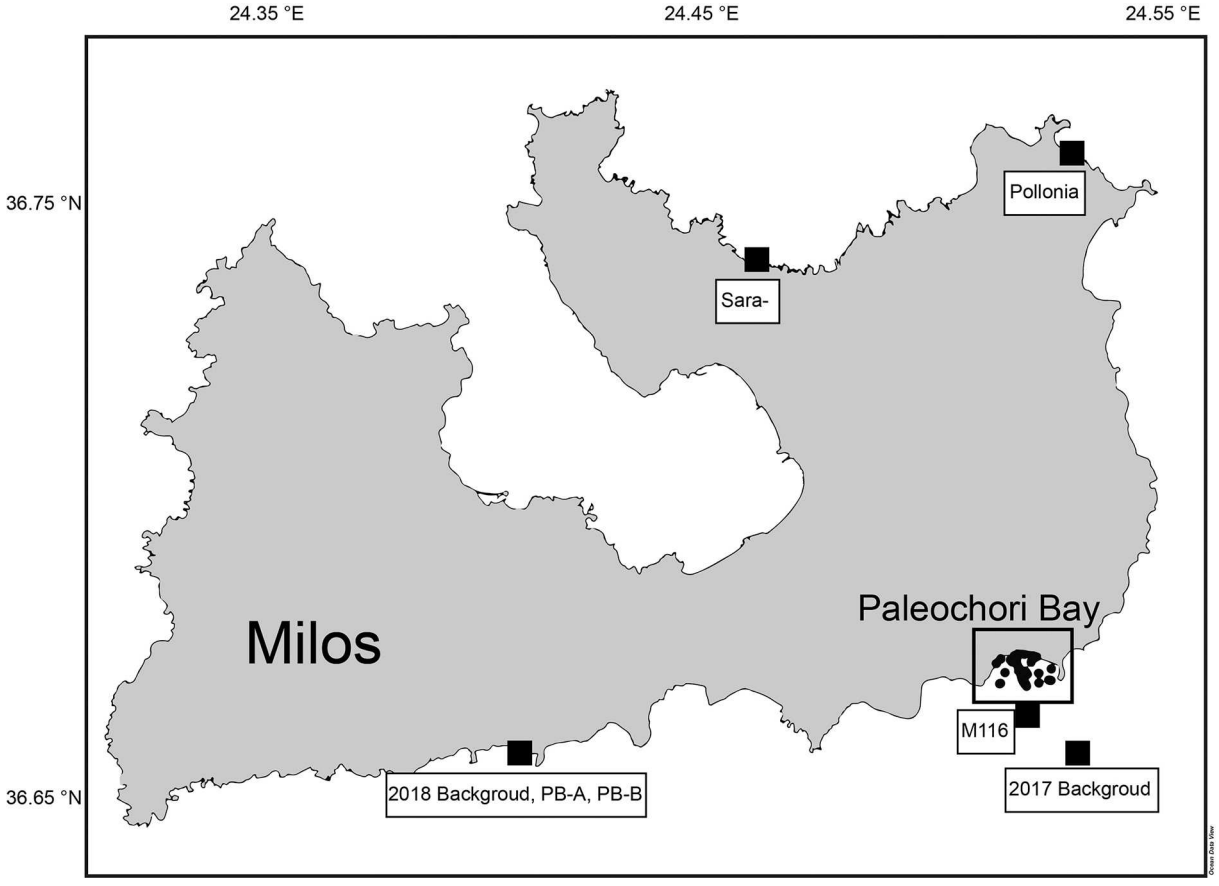

Fig. 1. Map of Paleochori Bay and locations around Milos Island, where Hg samples were collected. The map was generated by Ocean Data View.

basement (Papachristou et al., 2014). The bay contains numerous hydrothermal fluid and gas discharge areas and is one of the world's largest marine shallow-water hydrothermal systems (MSWHS). Two geothermal reservoirs were identified beneath the island: a high enthalpy system of up to 350 °C in the metamorphic basement and an overlying low enthalpy system of up to 175 °C within rhyolitic lavas close to the surface (Naden et al., 2005; Papachristou et al., 2014).

Hydrothermal fluids in Paleochori Bay are enriched in various heavy metals and gases are primarily composed of CO_2, CH_4, H_2S, and H_2 (Botz et al., 1996; Dando et al., 1995; Fitzsimons et al., 1997; Price et al., 2013a; Stüben and Glasby, 1999; Valsami-Jones et al., 2005). Previously, hydrothermal fluids were grouped into low- and high-Cl types resulting from phase separation in the subsurface, additionally characterized by high temperatures in porewaters, low Mg, and SO_4 concentrations in comparison to seawater (Papachristou et al., 2014; Price et al., 2013a; Valsami-Jones et al., 2005). In both cases, the emitted fluid was considered a mixture of seawater, water-rock interaction modified seawater, and magmatic water (Dotsika et al., 2009; Pflumio et al., 1991; Price et al., 2013a; Valsami-Jones et al., 2005). Hydrothermal activity is present throughout the bay; however, its frequency is most significant in the west (Khimasia et al., 2021). The volume of emitted gas and fluid in the bay was variable both temporally and spatially (Aliani et al., 1998; Botz et al., 1996; Dando et al., 1995; Miquel et al., 1998; Naden et al., 2005). Previous studies have linked low and high chloride fluids to phase separation and subsurface boiling (Price et al., 2013a; Valsami-Jones et al., 2005). However, recent findings suggested that subsurface transport could also be responsible for differing chemical compositions (Khimasia et al., 2021). Fluids were hypothesized to follow two different pathways, where greater permeability resulted in more substantial arc magmatic fluid influence and a secondary shallower pathway with meteoric water contributions.

In areas where hydrothermal discharge is present, the sediments are characterized by the occurrence of yellow-orange, white, or brown mats, hosting chemolithotrophic sulfur-oxidizing and sulfate-reducing bacteria (e.g., Yücel et al., 2013) (Fig. 2). The sediments may also appear red to yellow due to the precipitation of hydrous ferric oxides and arsenic sulfides from the hydrothermal fluids (e.g., Godelitsas et al., 2015) (Fig. 2). Voudouris et al. (2021) reported the presence of cinnabar (HgS) and arsenian pyrite (FeS_2) in areas with increased gas venting. Mineral precipitation and microbial growth generally are controlled by steep redox gradients at the sediment-water interface and fueled by rising hydrothermal fluid (Price et al., 2013a; Price et al., 2013b; Sievert et al., 1999; Wenzhofer et al., 2000; Yucel et al., 2013).

2.2. Methods

2.2.1. Field sampling

Fieldwork was conducted in June 2017, October 2018 and June 2020. The absence of wind or prevailing northerly winds prevented circulation patterns and wave action within Paleochori Bay during fieldwork, as discussed by Khimasia et al. (2021). Scuba divers did not observe any current while sampling. A total of 95 samples were collected across the bay and around the island for Hg (filtered and unfiltered, i.e., Hg_{diss} and THg), with select samples also analyzed for As, cations, and anions (Table 1, Appendix A). Most samples were a part of a larger dataset to estimate diffusive hydrothermal flux within Paleochori, including additional isotopic (δ^2H, $\delta^{18}D$) measurements (Khimasia et al., 2021). Eight samples representative of different environmental

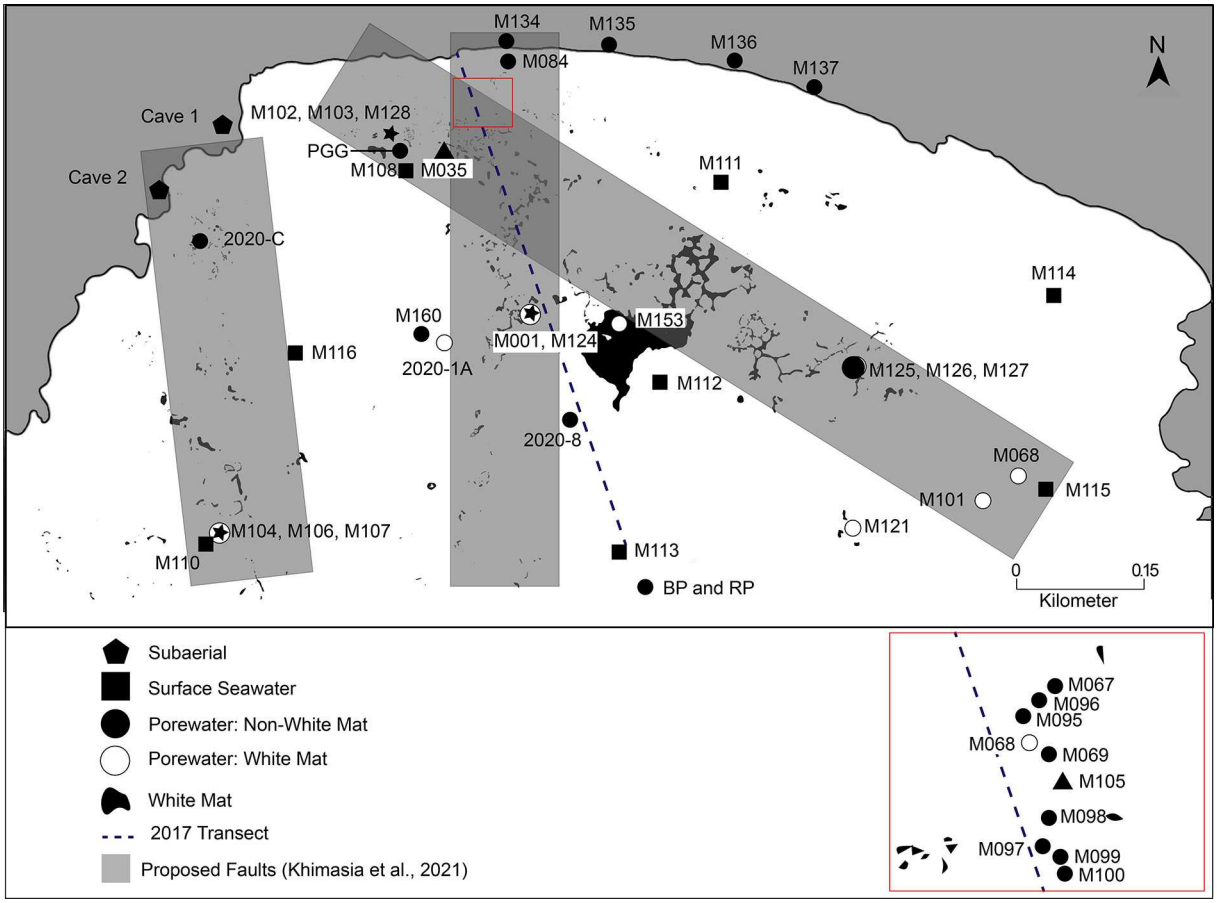

Fig. 2. Map of sampling points in Paleochori Bay. The red box was an area of numerous porewater samples with numerous areas of white mats and precipitates. The map was adapted from Khimasia et al. (2021). The dashed line depicts the surface and bottom water transect sampled in 2017. (For interpretation of the references to colour in this figure legend, the reader is referred to the web version of this article.)

Table 1
Average values for chemical composition and temperature for seawater and porewater by sample grouping.

Sample		T °C	pH	Cl mM	Br mM	SO_4 mM	As µM	Ca mM	Fe mM	K mM	Li mM	Mg mM	Mn mM	Na mM	Si mM	*Sr* mM	H_2S µM	THg pM	Hg_{diss} pM
Seawater																			
	Outside P.B.							29		56	3	31		553	2	0.2		3	
	Inside P.B.	20	8.1	637	0.9	33	0.0	11	0.0	11	0.4	54	0.0	520	0.0	0.1		5	6
Porewater																			
	Subaerial	91	3.4	754	1.1	23		16	0.8	24	2	20		277	4	0.2		2534	0.4
	Sand and Precip.	59	6.1	781	1.0	25	9	25	0.1	45	2	41	0.1	634	1.1	0.2	166	313	6
	White Mats	75	5.5	744	1.0	22	4	26	0.1	45	2	37	0.1	598	2	0.2	301	219	10
	Point Sources	114	6.5	605	0.9	31	0.2	11	0.0	11	BDL	52	0.0	506	0.2	0.1	4	1131	146
	Large Volume	97	5.7	889	1.1	20	35	30	0.1	61	2	35	0.1	688	2	0.3	1.0	37	2
	Brines	101	3.9	699	0.9	6		54	0.3	110	7	16	BDL	739	3	0.4		19	4

conditions such as sedimented, un-sedimented, seagrasses, white mats were selected for Hg speciation. Six of the eight samples included THg analysis of emitted gases. Point sources from Paleochori Bay were selected based on gaseous exhalations or fluid chemistry (Table 1, Fig. 3). Background seawater samples were collected in areas with no visible hydrothermal activity from outside of Paleochori Bay. In 2017, surface and bottom waters were collected simultaneously to determine dissolved Hg along a transect perpendicular to the beach progressing from shallow (approx. 1 m) into deeper water (approx. 15 m). Samples were collected at the surface and the bottom of the water column simultaneously, with surface divers collecting GPS data. In 2020 sediment and porewater samples were collected simultaneously at three locations representing non-hydrothermal (background) and hydrothermal areas (2020-1A, 2020-C and 2020–8).

Fluids were collected using samplers constructed from PTFE tubing and 10 mL pipette tips at 10 cm depth using polypropylene 60 mL syringes. Porewater temperatures were monitored at the depth of the pipette tip. No large deviations in temperature were permitted as sampling was performed to ensure that samples were not contaminated with seawater.

The pH (Halo Wireless pH meter, Hanna Instruments), conductivity and ORP (Myron Ultrameter) were immediately determined in the field. The samples were filtered through a 0.45 µm membrane, and the subsamples for trace elements and major cations were preserved with 2% (m/v) concentrated nitric acid.

2.2.2. *Mercury analyses*

Total Hg samples were collected unfiltered and filtered (0.45 µm) and analyzed following the USEPA (2002) protocol with a Brooks Rand CV-AFS analyzer in duplicate. In preparation for the analysis, 40 mL of the sample were added to a 60 mL Volatile Organic Analysis (VOA) glass vial with a PTFE-lined cap. Then 400 µL acidified bromide/bromate, a 1:1 mixture of 0.01 M bromide/bromate solution (Tritrisol, Merck) and 32% hydrochloric acid (Optima grade, Fisher Scientific) were added to the sample, and the light-yellow colored solution was left standing for at least 30 min at room temperature. The bromine chloride reactivity was

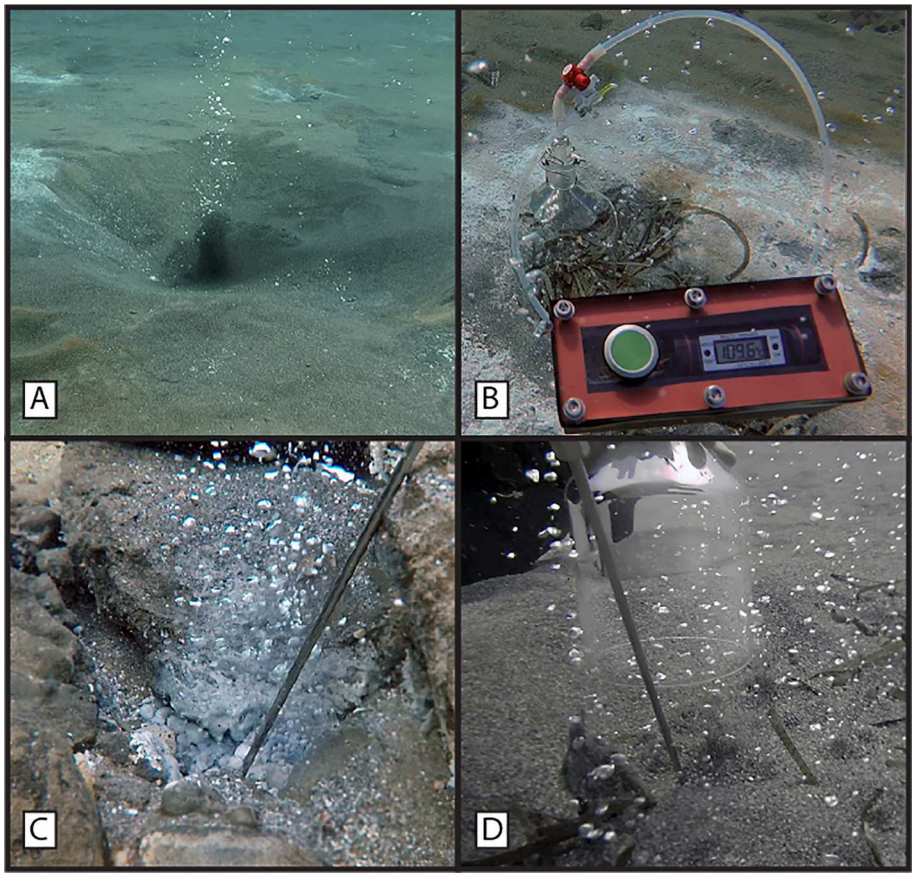

Fig. 3. Examples of features of the submarine hydrothermal system within Paleochori Bay. A) Highly sedimented site (M102). Significant gas exhalations throw sediment into the water column and only coarser grains remained. B) Highly sedimented with white mat and precipitate accumulations on the sediment surface with porewater temperature probe and gas collection funnel. C) Site without sediment cover (M103) with significant gas exhalations. No sediment remained at the point of emission. D) Low to moderate sedimentation (M125) of only a few cm. Multiple smaller but continuous gas exhalations were collected by the gas funnel when the image was taken.

then quenched by the addition of 100 µL 30% (m/v) hydroxylamine hydrochloride solution (ReagentPlus, 99%, Sigma-Aldrich) and shaken. Elemental Hg was produced in the solution by adding 200 µL of a 20% (m/v) tin(*II*)chloride solution (Reagent grade, Alfa Aesar). The detection limit for this method was determined to be 0.04 ng/L ($n = 10$) for our laboratory. The certified reference material ORMS-5 (elevated Hg in river water, National Research Council Canada) was used for quality control. The reference material was certified for a concentration of 26.2 ± 1.3 ng/L T-Hg and measured within 5% of certified values.

The sediment samples were digested in 10:1 aqua regia following Bloom et al. (2003) and THg was analyzed by CV-AFS. The certified reference material PACS-1, certified for a concentration of 4.57 ± 0.16 µg/g THg was used for quality control.

Volatile Hg was collected by purging 1 L of hydrothermal fluid with Hg free nitrogen onto gold and carbo traps and analyzed by CV-AFS (Cossa et al., 2011; Lehnherr et al., 2011).

Analysis of MeHg was carried out by species-specific isotope dilution gas chromatography. A 100 mL sample was spiked with a $Me^{201}Hg$ solution (ISC Science, Spain) and left equilibrating for an hour. An optimal ratio of 4.25 for $Me^{201}Hg$ in the spike to $Me^{202}Hg$ in the sample was the spiking aim. Based on the assumption of 5% of T-Hg being present as $Me^{201}Hg$, the amount of the enriched isotopic solution was calculated for the initial spiking. An acetate buffer, prepared from trace metal grade acetic acid (Fisher Scientific) and 30 M NaOH (Suprapur, Merck), was added to the sample. The pH was adjusted to 3.9 with sodium hydroxide solution (30 M, Suprapur, Merck). Subsequently, 1 mL propylation reagent (1 g sodium tetra-propyl borate (Merseburger Spezialchemikalien, Germany) in 100 mL oxygen-free Milli-Q water) was added to the sample followed by 200 µL n-Hexane (Reagent Grade ACS, Riedel-de-Haen). The Hg species were extracted into the n-hexane phase by shaking for 10 min, and the n-hexane phase was taken out for analysis by gas chromatography coupled to ICP-MS (Element 2, Thermo Scientific) with an in-house-built heated transfer line (temperature of 160 °C). A cyclonic spray chamber was attached at the transfer line just before the ICP torch for wet plasma conditions giving the option of plasma tuning and monitoring with an internal Thallium standard.

Gas samples were collected into Tedlar© bags using a custom-built glass funnel connected to Teflon tubing in combination with a standard lift bag. The lift bag was attached to lead weights, which enabled the calculation of gas volume collected, i.e., the volume of gas needed to displace enough seawater to lift the bag at a given depth and lead weight. To remove sulfur species from the gas, the samples were passed through an alkaline solution. The sample was then trapped in a 0.5 M permanganate solution in 2 N sulfuric acid and analyzed on the CV-AFS as THg (Brombach and Pichler, 2019). Exact rates of emission were not calculated; however, relative rates were established based on gas sample retrieval time. For simplicity, low emission samples required more than 30 min of dive time, and high emission samples needed less than 30 min. Each gas sample site was named (Fig. 3) and chosen based on visible physical characteristics (see Table 2, Fig. 3).

Table 2
Named gas emission sites with descriptors.

Site	Emission Rate	Sediment Coverage	Descriptor
Red	Low	High	White mats and red metal precipitates surrounding
Seagrass	Low	High	White mats and seagrass growth surrounding
Crater	High	High	Sand covered by black precipitates
Eastern	Low	Medium	No white mats or metal precipitates, easternmost gas sample taken
Screamer	High	Low	No sediment coverage, cave-like structure above gas emission point
Boulder	High	Low	No sediment coverage, gas emitted from between two boulders

2.2.3. Other measurements

Anions were analyzed in a non-acidified, filtered sample (0.45 µm) using a Metrohm 883 Basic IC instrument with a 5 µL injection loop and a Metrosep A Supp5 (150 × 4.0 mm; 5 µm) column. Quality control samples were an internal standard and IAPSO, an artificial seawater. Major cations and some trace elements were measured by inductively coupled plasma-optical emission spectrometry (ICP-OES) using a Perkin Elmer Optima 7300 DV instrument. The detection limit for most elements was around 1 to 10 µg/L, which was not sensitive enough for trace elements but sufficient for the major elements present in the sample. All water samples were diluted by a factor of 100 due to the high salinity of the samples. Quality control was assured with different certified waters: EnviroMAT Groundwater Low (ES-L-2) and High (ES-H-2), both from SCP Science, Canada, are groundwater samples while CRM-SW (High Purity Standards, USA) was a certified seawater.

Trace elements were analyzed with inductively coupled plasma mass spectrometry (ICP-MS, Element 2 Thermo Scientific). The mass analyzer of the Element 2 instrument is based on a magnetic and electric sector field. Mass interference based on polyatomic and isobaric interference can be overcome by adjusting the mass resolution from low to high, which is essential for some trace elements, e.g., arsenic. The same principle for sample dilution for saline samples as was described for ICP-OES. Plasma fluctuations were monitored via the addition of internal standards to each sample.

2.2.4. Flux calculations

The flux (pmol/m^2/h) of Hg^0 to the atmosphere from each of the sampling sites was calculated using equations by Liss and Slater (1974) (1) and Wanninkhof (1992) (2), as implemented by Wängberg et al. (2001). Where k_w (cm/h) is the gas transfer velocity, u_{10} is the wind speed at 10 m height, Sc_{Hg} is the Schmidt number for Hg in seawater and Sc_{CO2} is the Schmidt number for CO_2 in seawater (Kuss et al., 2009), and H′ is Henry's law constant. An approximate value was used for atmospheric Hg (7.5 pmol/m^3), and the percent volatile Hg^0 was assumed to be 10% of Hg_{diss} (Horvat et al., 2003). Schmidt numbers 689 for Hg and 660 for CO_2 were used.

$$Flux\ to\ the\ Atmosphere = k_w \left(DGM - TGM/_H \right) \quad (1)$$

$$k_w = 0.31\ u_{10}^2 \left(Sc_{Hg}/Sc_{CO2} \right)^{-0.5} \quad (2)$$

Samples were plotted against Na/K ratios, which have been used to indicate rapidly rising fluids (Henley, 1995) and, more recently, on Milos in conjunction with isotopic analysis (Khimasia et al., 2021).

3. Results

Conservative element data (Na, Cl, K, etc.) from porewaters and seawater samples were comparable to previously established mixing lines of hydrothermal fluid and seawater (Price et al., 2013a; Valsami-Jones et al., 2005). Samples taken at background sites in and outside Paleochori Bay were significantly lower in THg concentration than those influenced by hydrothermal activity (Table 1, Appendix A). All samples with a pH less than 4, temperatures above 65 °C, and Hg enrichment (THg and Hg_{diss}) were collected in Paleochori Bay.

Within Paleochori Bay porewaters, concentrations of Hg were highly variable between sampling sites. However, marked increases in the concentration were observed in hydrothermally influenced areas indicated by temperature, low Mg and high Cl concentrations. The high-Cl fluids of Paleochori Bay were found to contain low (< 15) Na/K ratios with a median value of 6.71 with isotopic values of δ^2H and $\delta^{18}O$ consistent with rapidly rising fluid (Khimasia et al., 2021).

3.1. Water samples

3.1.1. Seawater

Background seawater and samples taken outside of Paleochori Bay were comparable to previous studies concerning cations, anions, and Hg (Cossa et al., 1997; Horvat et al., 2003; Khimasia et al., 2021; Valsami-Jones et al., 2005). Within surface waters of Paleochori Bay, THg concentrations were higher than samples from outside of Paleochori Bay and background samples (Table 1, Appendix A). The concentration of all other elements (Cl, Br, SO_4, Ca, Fe, K, Li, Mg, Mn, Na, Si, Sr) measured showed little variation (0.29% to 6.5% RSD) between samples. It reflected control group concentrations apart from As, which was highly variable (77%).

Hg concentrations were highest near the shoreline for transect samples, where the known hydrothermal activity occurred directly beneath the sand surface (Fig. 4). Concentrations quickly returned to low pM values in surface and bottom waters but increased again when white mat accumulations were encountered (e.g., at approximately 0.3 km distance from shore, Fig. 4). Surface and bottom water samples were enriched by 314 to 18,759% over background Hg_{diss}.

3.1.2. Paleochori Bay vents, Porewater and sediment

Porewaters included high- and low-Cl fluids with strong relationships between known hydrothermal indicators of active areas (Khimasia et al., 2021). Porewaters from within Paleochori Bay contained low (17 pM) to high (2894 pM) THg concentrations with a maximum of 69% Hg_{diss} (Appendix A). Methylated and volatile species were all below detection limits. Hydrogen sulfide concentrations ranged from below the detection limit to 1.2 mM. Background porewater within Paleochori Bay contained 98 pM THg and 4 pM Hg_{diss}.

Water samples collected from the point sources (vents) shown in Fig. 3 showed significant chemical composition variations except for THg, Hg_{diss}, and Hg_{gas} (Appendix A). The Boulder and Screamer sites were collected at the point of emission at the sediment-water interface due to the rocky hard bottom at those sites and thus, seawater contamination was unavoidable.

In 2017 an additional sample was taken from a point source, which discharged at sea level in a small cave. That sample (Cave-1) had higher than seawater Cl and Na but lower SO_4 concentrations. The Cave-1 sample contained the highest measured concentration of THg for all samples (5066 pM), as well as the lowest pH (1.87).

The highest THg concentrations were associated with low Na/K ratios (Fig. 5). High Na/K ratios (> 15) were related to low-Cl fluid and low Si concentrations. The percentage of Hg_{diss} was more significant in high Na/K ratio samples.

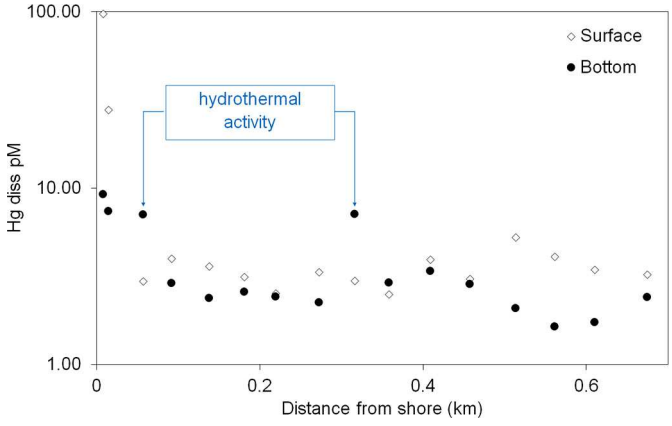

Fig. 4. Transect of total Hg in filtered samples for the transect of surface and bottom samples in Paleochori Bay done in 2017. Surface samples were generally higher, except immediately adjacent to the shore and where hydrothermal activity was observed (i.e., white mats). The exact location of the transect is given in Fig. 2.

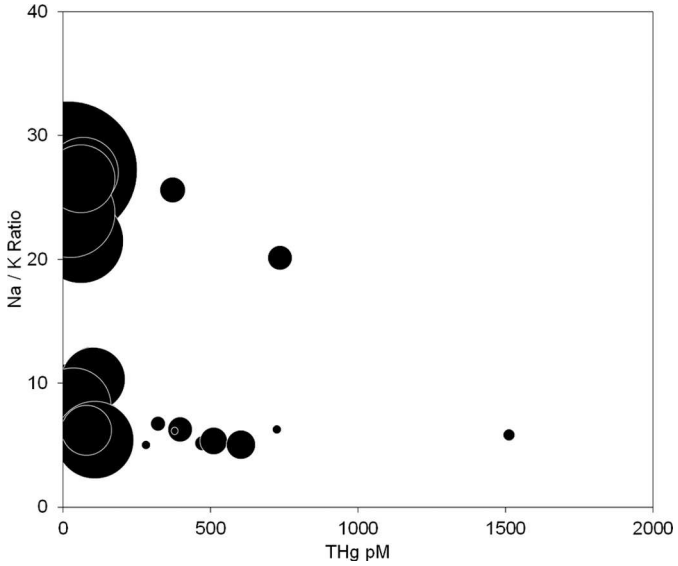

Fig. 5. Total Hg (THg) concentration in porewaters vs Na/K ratios. The area of the circle corresponds to the percent dissolved Hg in the sample. Lower (< 15) Na/K ratios were associated with rapidly rising fluid along fault lines.

Data for THg of the three sediments samples and their corresponding porewater concentrations are presented in Table 3. Compared to the two hydrothermal samples, the "non-hydrothermal" sediment sample had higher THg in the porewater and lower concentration in the corresponding sediment, 97.9 pM and 414 pM/g. The background porewater sample's chemical composition was similar to seawater, and the area of sampling showed no physical indicators of hydrothermal activity.

3.1.3. White patch flux calculations

White patch fluid flux calculations of Hg were completed using minimum and maximum concentrations of both total and dissolved Hg (347 to 777 μM/day THg, 51 to 210 μM/day Hg_{diss}) and flux estimates as described in Khimasia et al. (2021).

3.2. Gases

Gas concentrations of Hg were highly variable (0.7 to 2792 nmol/m^3), and no statistical or otherwise significant relationship could be observed between Hg in gas and porewater. Elevated Hg in the gas phase did not necessarily indicate high or low Hg concentrations within the fluid phase and vice versa. However, the highest Hg concentrations in the liquid phase were observed at locations with intense gas emission, although intense gas emissions did not indicate high Hg concentrations within the gas phase (e.g., Crater site). However, it seemed that the absence of a sediment cover at the sampling site was responsible for higher Hg_{gas} concentrations (Fig. 6).

Dando et al. (1995) estimated the release of 0.21 to 1.05 × 10^{11} mol per year of total gas. Based on this estimation, the contribution of Hg from the MSWHS to Paleochori Bay was calculated to be 3.3 × 10^{-4} to 6.6 mol Hg per year.

Table 3
Sediment and porewater concentrations collected in 2020.

Sample	Temperature °C	pH	THg pM	Hg_{diss} pM	Sediment THg pmol / g
2020–8	22	7.72	97.9	3.7	414
2020-C	86	1.87	23.7	5.0	1213
2020-1A	52.7	5.35	78.2	5.2	917

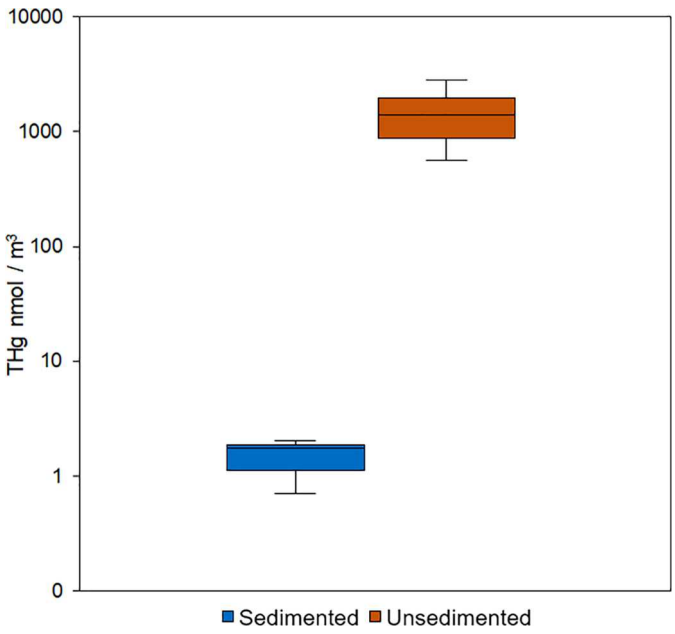

Fig. 6. Concentration of total mercury (THg) in the gas phase. Sedimented sites are in blue and sites without a sediment cover are in orange. (For interpretation of the references to colour in this figure legend, the reader is referred to the web version of this article.)

4. Discussion

4.1. Hg concentrations within the water column

Our data showed elevated total and dissolved Hg concentrations in Paleochori Bay compared to seawater unaffected by hydrothermal activity. Background concentrations of Hg for the Mediterranean are known to be in the low pM range. For example, Cossa et al. (1997) and Horvat et al. (2003) showed concentrations of THg ranging from 0.5 to 4 pM in the Western Mediterranean. The ratio of dissolved Hg to THg is elevated in open ocean Mediterranean waters (from 32 to 95%) due to the low abundance of particulate matter (Horvat et al., 1999). Surface waters collected from Milos outside of Paleochori Bay were lower than average Mediterranean values.

In contrast, surface water THg samples from Paleochori were enriched by over 3000% (15.4 pM) than this study's assumed background concentration (0.5 pM). The highest concentrations of THg in surface water were located above areas of known shallow-water hydrothermal activity in the western portion of Paleochori Bay (Fig. 2, Appendix A). The transect, where bottom and surface waters were sampled simultaneously (Fig. 4), showed that surface water was generally elevated above bottom water, except at two locations where hydrothermal activity was present (Fig. 4). At a distance of approximately 60 and 300 m, elevated Hg concentrations were observed in bottom waters associated with a white mat. The high concentrations at the beginning of the transect are not considered representative because of substantial mixing within the surf zone and due to a shallow water depth of less than 1 m. Warm hydrothermal fluids are buoyant relative to seawater. Therefore, they are known to rise and transport trace metals to the sea surface, resulting in higher surface water concentrations than in the bottom water (Pichler et al., 2019; Pichler et al., 1999b). This overall strongly suggests hydrothermal emissions are a source of Hg to Paleochori Bay. The extent of this cycling may be restricted to local rather than regional areas. Therefore, the speciation of Hg from the pore fluids holds vital information on the fate of the Hg discharged.

4.2. Hg concentrations in Porewaters and sediments

The transformation of inorganic mercury to methylated species was negligible. Sub-optimal methylation conditions in the shallow subsurface (e.g., > 75 °C, up to 1200 μM H_2S, < 18 pM Hg_{diss}) likely prevented appreciable MMHg and DMHg accumulation (Bayraktarov et al., 2013; King et al., 2000). Methylation rates under optimal conditions generate approximately 1 to 2% MMHg of THg (King et al., 2000). Therefore, concentrations of up to 12 pM would be expected for Paleochori Bay porewater, well within the detection limit of the method. However, MMHg was not detected in any sample.

Relationships between Hg (THg and Hg_{diss}) and typical hydrothermal indicators (e.g., Cl, temperature, SO_4, etc.) were observed in areas without white mats. However, areas with white mats did not share these relationships. In particular, a significant positive trend (nonlinear) between THg and temperature was observed in areas without white mats (see Fig. 7A). Even by removing a single high THg sample (Crater site), the trend was maintained for the data, with an inflection point around 75 °C, where the slope increased significantly. Frequently used as an indicator of hydrothermal influences, a positive trend with THg concentrations is intuitive. However, this relationship was not present in the white mat areas, suggesting some removal mechanism or lack of an enriched Hg source, particularly at higher temperatures.

Porewaters enriched with Hg were also enriched with arsenic, a metalloid extensively linked to hydrothermal activity (e.g., Pichler et al., 1999c; Price et al., 2013a). A significant positive correlation was observed between THg and As concentrations in areas without white mats. Mercury and As both belong to the so-called "epithermal suite" of elements (Au, Ag, Te, Se, Hg, As, Sb, and Tl) (Berger and Eimon, 1983; Saunders and Brueseke, 2012; Saunders et al., 2008). Two main chemical properties of the "epithermal suite" of elements appear to control their similar behavior and common occurrence: (1) they are all "soft" Lewis acids, meaning they form covalent bonds with "soft" Lewis bases such as H_2S, S^{2-}, etc., and (2) they all have similar volatility, explaining why they are liberated together from the mantle. Enrichments of "epithermal elements" in vent fluids were identified in several MSWHS (Gamo and Glasby, 2003; Johnson and Cronan, 2001; McCarthy et al., 2005; Prol-Ledesma et al., 2004), making them excellent targets for Hg analysis. This was also confirmed for Paleochori Bay by Voudouris et al. (2021), who reported the presence of cinnabar within arsenian pyrite layers in areas with hydrothermal activity.

As a class b soft metal, Hg will more likely travel with sulfide ligands within shallow, low enthalpy systems, with vapor transport more likely within deeper, high enthalpy systems (Barnes and Seward, 1997; Barnes, 2015). Soft metal complexes are less sensitive to temperature changes, with deposition more likely with oxidation, dilution and pH. Chemical pathways of Hg within the subsurface of New Zealand hydrothermal environments were described in detail by Christenson and Mroczek (2003). As liquids and gases traveled through the upflow zone, precipitation of Hg as cinnabar, or coprecipitation with pyrite, occurred from liquids and directly from gases. As a result of changes in pH, Eh and temperature gas condensation happened and resulted in precipitation of said minerals causing the complete removal of THg from the gas phase. In gas-brine interactions, Hg behavior was strongly linked to heating and cooling regimes within the subsurface. Upon mixing with overlying oxygenated water, Hg_{gas} was oxidized by sulfur or oxygen to form Hg—S species or Hg—Cl species. This oxidation step removed volatile Hg species and flux to the atmosphere was limited.

The primary difference between white mat and non-white mat sample areas, in terms of sulfur concentration, is the balance of oxygen penetration into the shallow subsurface and hydrogen sulfide production, paired with large fluxes of an H_2S-rich hydrothermal fluid. In previous studies, areas of high temperatures without white mats promoted increasing oxygenation of the subsurface and production of elemental sulfur from hydrogen sulfide, limiting S bioavailability (Wenzhofer et al., 2000; Yucel et al., 2013). The sensitivity of Hg—S

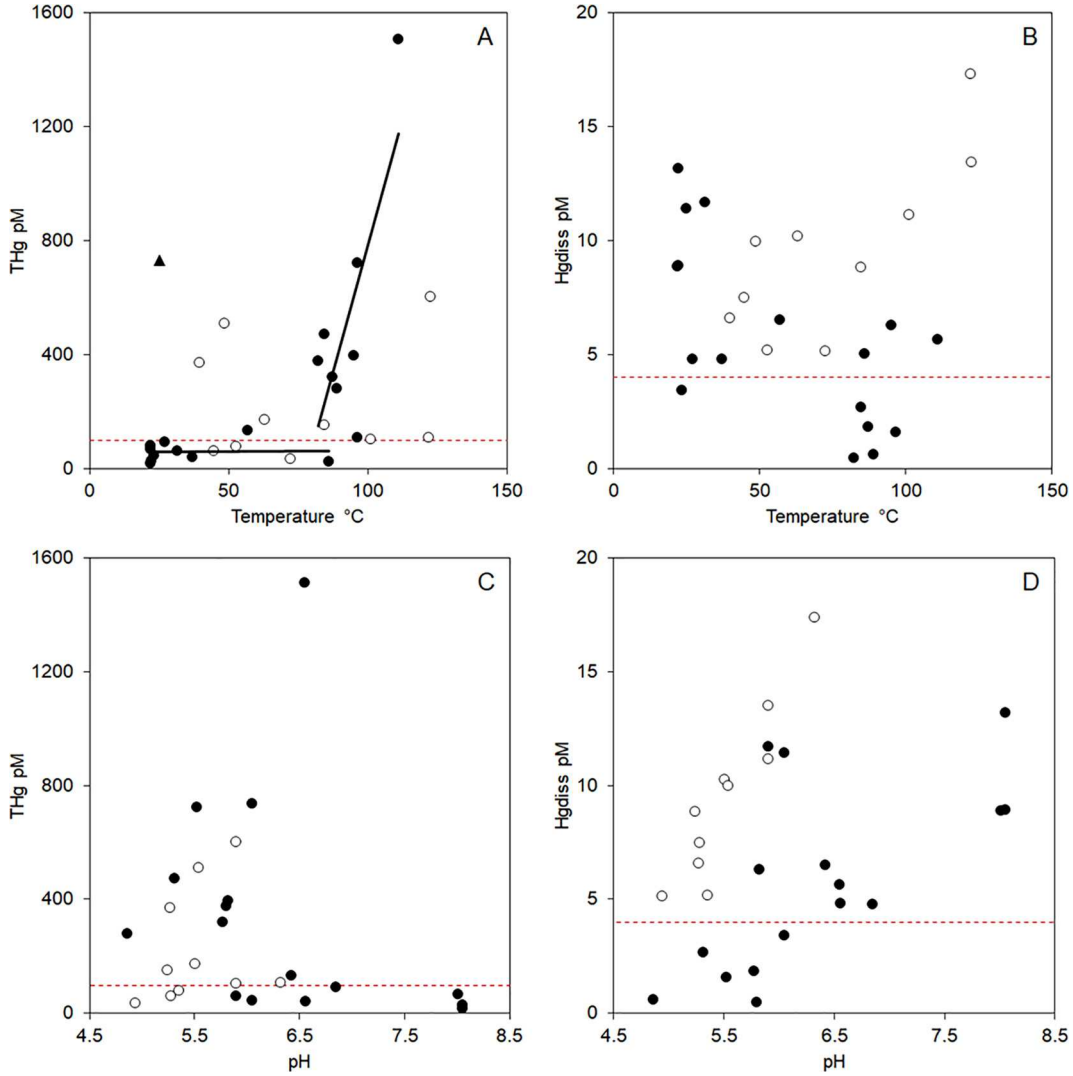

Fig. 7. Scatterplots of THg and Hg_{diss} vs temperature (A and B) and pH (C and D). Samples from areas of white mat accumulations in white circles, non-white mat samples in black. Horizontal red lines represent background porewater concentration in THg and Hg_{diss} respectively. Black lines in (A) represent linear fit slopes of THg in non-white mat areas above and below 75 °C. The black triangle represents a sample with possible contamination or entrainment of a Hg rich precipitate. (For interpretation of the references to colour in this figure legend, the reader is referred to the web version of this article.)

minerals to temperature changes follows known thermodynamic patterns established by Barnes et al. (1967). Areas with white mats provided enough flux of H_2S to sustain microbial activity while minimizing contamination with oxygenated seawater. Given those considerations, the effect of temperature on THg in non-white mat areas is more likely associated with hydrothermal fluid flow. This effect was seemingly masked in the shallow subsurface beneath white mat areas. There H_2S did not oxidize to SO_4 and thus could have resulted in HgS formation as discussed for aquatic environments by Hsu-Kim et al. (2013). This behavior has been similarly established for iron sulfide formations (Pichler et al., 1999a) and plays a substantial role in Paleochori Bay. The variations observed between samples of similar chemistry, geological location, or environmental conditions are indicative of a system precipitating Hg within the shallow subsurface and at the sediment-water interface.

Many porewater samples, although from hydrothermal areas, contained less THg than what is considered the background concentration of 98 pM (Fig. 7A), which would indicate that the source of the hydrothermal fluids could have been depleted in Hg (e.g., brine phase, meteoric water or seawater) and that any influence of potentially enriched sources (e.g., condensed vapor phase or gases) was limited. On the other hand, removing Hg in the shallow subsurface could have happened due to precipitation or scavenging. The majority of THg was bound to particles, as shown by the low Hg_{diss} concentrations in most porewater samples (Appendix A). Thus, hydrothermal solutions enriched in elements known to scavenge Hg, such as sulfur species, could therefore be depleted in THg compared to the background site. This has been observed in the water column in deep-sea plumes (e.g., Bowman et al., 2016), in the outflow from hot springs, where the oxidation of Hg^0 led to the precipitation of Hg—S minerals (Davey and van Moort, 1986) and in Paleochori Bay. Voudouris et al. (2021) reported grains of cinnabar up to 3 μm in size in arsenian pyrite layers. The pyrite precipitation was associated with high-Cl fluids. Indeed, the sediment sample from the hydrothermal site 2020-C had the highest THg, while its corresponding porewater had the lowest THg concentration relative to the other two sediments (Table 3).

The high THg concentrations observed in Paleochori Bay porewaters were related to low Na/K ratios, indicating a rapidly rising hydrothermal fluid along fault lines (Khimasia et al., 2021). Br/Cl ratios from all pore fluid samples from Paleochori Bay were comparable to those described by Valsami-Jones et al. (2005) and Price et al. (2013a) for this system. Based on Br/Cl ratios, subcritical phase separation was

suggested as an essential subsurface process. As discussed in (Khimasia et al., 2021; Wu et al., 2011), this ratio does not necessarily define samples as representative of vapor or brine phases. The THg and Hg_{diss} in samples collected from hydrothermally active areas were generally above background porewater concentrations regardless of high or low Cl values. However, samples with higher THg were generally high-Cl fluids. Additionally, those samples with low Na/K ratios contained the highest THg concentrations (see Fig. 5). Those samples corresponded to the ones described by Khimasia et al. (2021), which trended towards arc magmatic water. That was unsurprising given that various samples collected on land also indicated a magmatic fluid component in the Milos hydrothermal system (e.g., Dotsika et al., 2009).

One surprising aspect of porewater fluids sampled on Milos was the low ratio of Hg_{diss} to THg for most samples. If near-surface phase separation were happening, high concentrations of THg would be expected in low-Cl fluids. On the contrary, higher THg concentrations were observed in high-Cl samples, with high Hg_{diss} ratios in low-THg and low-Cl samples. A notable exception being the Eastern point source, where a relatively strong gas emission was also present, potentially influencing Hg_{diss} concentrations.

Papachristou et al. (2014) described the Milos system as containing two geothermal reservoirs, a deep high enthalpy system and a shallow (< 150 m below surface) lower enthalpy system with temperatures between 50 and 100 °C. The geothermal gradient is high in the island's central and eastern areas, with the low enthalpy system primarily associated with the central Vounalia area. Condensation of Hg^0 from hydrothermal vapors would fall within the temperature range of the low enthalpy system, where concentrations may be high (e.g., Davey and van Moort, 1986; Migdisov and Bychkov, 1998). The lack of Hg^0 within samples, coupled with high ratios of particle-bound Hg species, indicates that assuming low-Cl fluids result from a condensed vapor phase, Hg would be removed from solution before emission, potentially due to oxidation in the shallow subsurface. The high ratios of particulate bound Hg in high-Cl fluids with low Na/Cl, coupled with the isotopic data described in Khimasia et al. (2021), point towards a rapidly rising deep-seated hydrothermal fluid to be the primary source of Hg to Paleochori Bay.

4.3. Diffuse flux modeling

Diffusive flux modeling assumed THg and Hg_{diss} from 10 cm depth to be transported to the water column. However, as discussed above and as observed by Lamborg et al. (2006), removing Hg before emission is possible. Discharge through sediments can effectively remove Hg and other metals from hydrothermal fluids (e.g., Leal-Acosta et al., 2010; Pichler et al., 1999a; Pichler and Veizer, 2004; Price and Pichler, 2005). Besides, scavenging in hydrothermal plumes can be an important process for Hg speciation and sedimentation (Bowman et al., 2015). Nevertheless, the transect showed increases in Hg_{diss} in bottom water where white mats were noted (Fig. 4). This supports diffusive flux as a contributor to water column Hg_{diss} concentrations despite the potential for precipitation.

The minimum estimated daily flux from the white mat areas of 347 μM THg and 51 μM Hg_{diss} was far higher than the estimated daily flux of Hg^0 to the atmosphere of 0.76 μM. An average elemental Hg flux of 1.3 pmol/m^2/h to the atmosphere, with a maximum flux of 2.7 pmol/m^2/h, was calculated (Table 4). This flux is similar to estimates observed for some Panarea sites, e.g., 3.48 pmol/m^2/h at Bottaro North (Bagnato et al., 2017) and the open waters of the Mediterranean and polluted coastal areas (e.g., 3.99 to 25.9 pmol/m^2/h, respectively) (Andersson et al., 2007). It should be noted that estimates on flux values would vary significantly based upon deviations from the assumed 10% Hg^0 speciation of Hg_{diss}. However, even if all Hg_{diss} would be present as a volatile species, this would result in only a 10-fold increase in flux. Without substantial increases in wind speed coupled with high volatile Hg concentrations, the flux of Hg to the atmosphere cannot balance the diffusive flux of Hg to the system. Some portion of Hg must, therefore, be removed before venting.

Table 4
Surface water concentrations and flux to the atmosphere.

Sample	Temperature °C	pH	GPS Lat	GPS Lon	THg Filtered pM	Flux pmol / m^2 / hr
M108	20.1	7.87	36.67371	24.51567	4.2	2.7
M109	20.1	8.11	36.67180	24.51420	1.4	0.9
M110	20.1	8.19	36.66983	24.51301	0.7	0.4
M111	20.1	8.03	36.67359	24.51989	2.1	1.3
M112	20.1	8.05	36.67150	24.51904	1.3	0.8
M113	20.1	8.14	36.66973	24.51851	1.7	1.0
M114	20.1	8.01	36.67241	24.52428	3.3	2.1
M115	20.1	7.99	36.67040	24.52418	2.1	1.3
M116	20.1	8.01	36.66472	24.51906	1.5	0.9

4.4. Point sources

The complexity of the hydrothermal system in Paleochori Bay concerning Hg was highlighted by the heterogeneity of the point source samples. Valsami-Jones et al. (2005) concluded that subaerial low Cl and Mg fluids were likely representative of an end-member equilibrated at depth. Additionally, Price et al. (2013a) concluded low Cl fluids were resultant from condensed vapor phases with some mixing of seawater and the brine phase.

The Cave-1 fluid contained elevated cations, anions, and metals, including the highest THg measured in the study (5066 pM). This sample was collected closer to high-temperature areas observed in Paleochori Bay (Khimasia et al., 2021). Enrichment of Cl, depletion of Mg, and low pH indicated a strong influence of hydrothermal fluid. The Cave-1 sample is indicative of a high THg arc magmatic water. Simmons and Brown (2007) described Hg concentrations from deep hydrothermal solutions in New Zealand, an area of known high hydrothermally sourced Hg. Concentrations ranged from 3400 pM to over 400 nM in hydrothermal fluids ranging in temperature from 195 to 322 °C.

Despite sampling difficulties, the extreme enrichment of THg from the Eastern, Boulder, and Screamer sites warranted further investigation. These fluid samples are likely better representations of the localized impact of hydrothermal fluid on seawater based upon fluid chemistry and sampling environment.

The Eastern Site was moderately sedimented and contained the lowest THg and Hg_{diss} concentrations of the three. Despite a high porewater temperature (122 °C), pH remained close to neutral (6.04). The depleted cation and anion concentrations of the Eastern sample indicate a contribution of a low-Cl fluid. With MMHg, DMHg, and Hg^0 concentrations below detection limits, the high concentration of Hg_{diss} was comprised entirely of Hg^{2+}. The depletion of cations and anions within the Eastern site fluid was slight, with SO_4 close to background values, indicating a strong influence of oxygenated seawater. The Na/K ratio of the Eastern site was high, and the site was located along proposed fault lines (Khimasia et al., 2021). However, the porewater concentration of THg was only moderately elevated compared to background porewater. If low Cl concentrations were caused by a condensed vapor phase, higher THg concentrations would be expected. Therefore, either the low Cl concentration was due to meteoric water, or THg was removed from the fluid before emission. Given that the sample's location lies on a fault line with a strong gas emission, the porewater's low THg is surprising. Further investigations into the area would be needed to understand the site further.

Like the Eastern site, the Screamer site contained high Hg_{diss} (217 pM) relative to THg (312 pM) and close to seawater concentrations of anions and cations. The Boulder site contained over twice the Hg_{gas} of the Screamer site and close to ten times the THg in the liquid sample. However, the Hg_{diss} concentration was comparable to that of the

Screamer site (115 pM). However, these sites had hard rocky bottoms where clean fluid samples could not be obtained. Instead, the Hg concentrations at these sites reflected a mixture of emitted pore fluid, seawater, and equilibrated gas. As was observed at the Eastern site, MMHg, DMHg, and Hg^0 were below detection limits; therefore, all Hg_{diss} was in the form of Hg^{2+}.

Above the Boulder and Screamer sites, THg values within surface waters were high (9.6 pM). The large quantity of point sources (Khimasia et al., 2021) along with the high concentrations of THg from fluid samples and overlying surface waters, indicates transport from the point source to the surface, as was observed for other metals from hydrothermal systems (Pichler et al., 2019; Pichler et al., 1999b). Measurement of surface waters directly above the Eastern site was not completed; however, the surrounding surface water sites were elevated compared to background samples.

With no visible fluid emission at the Boulder and Screamer site and major elements similar to local seawater values, the liquid samples taken from the point sources are hypothesized to be seawater primarily affected by hydrothermal gases. High THg and Hg_{diss} suggest rapid oxidation of Hg^0, the assumed primary Hg species within the gas, as was discussed in Christenson and Mroczek (2003).

4.5. Mercury in hydrothermal gases

Lower gas emission rates were observed at the Seagrass and Red sites, where Hg_{gas} concentrations were low. The low gas emission rates provide for increased subsurface reaction times and, therefore, the greater potential for removal (Bower et al., 2008; Christenson and Mroczek, 2003; Pichler et al., 1999a). However, given the gas sites' locations in relation to the proposed fault lines (Khimasia et al., 2021), high Hg_{gas} would have been expected.

The two highest Hg concentrations measured had limited sediment coverage (Boulder and Screamer sites). Both sites had high gas emission rates; however, the third high gas emission site (Crater) did not contain high Hg concentrations in the gas phase. This result was astounding given the low Na/K ratio and proximity to the Boulder and Screamer site. A large amount of overlying sulfur-rich sediment at the point of emission is hypothesized to be a primary removal mechanism for Hg_{gas}. The sediment cover acts as a filter for Hg species while at the same time facilitating the percolation of oxygenated seawater further into the subsurface due to the formation of circulation cells caused by the constant gas stream (e.g., O'Hara et al., 1994). The introduction of oxygen and subsequent oxidation of Hg^0 facilitates Hg removal, as described previously by Davey and van Moort (1986) for the Hg deposition at Ngawha Springs in New Zealand. The large concentration of Hg bound to particulates in the fluid phase compared to Hg_{diss} supports extensive scavenging at this site. The differences between concentrations in the fluid and gas phases are likely the result of rapid oxidation described by Christenson and Mroczek (2003).

5. Conclusions and summary

Elevated concentrations of THg within surface waters within Paleochori Bay were due to the contributions of hydrothermal fluids and gases in the form of diffusive flux and high THg point sources. We argue that these contributions must be substantial, given the potential for dilution and removal mechanisms (e.g., transport, sedimentation, atmospheric flux). The highest fluxes to the atmosphere were those closest to shore and associated with shallow water hydrothermal activity. At the same time, Hg_{diss} tended to be higher in samples with higher THg, while the Hg_{diss} fraction of THg did not. Direct measurement of volatile Hg^0 from the surface would be needed to measure this flux more accurately.

Environmental conditions commonly associated with Hg speciation and behavior, such as epithermal elements (As), scavenging species (S), and indications of hydrothermal activity (high temperatures, pH, salinity, emission site proximity) proved to be irrelevant outside of the specified sample groupings. Areas of white mat accumulation showed Hg_{diss} correlated with pH, while areas without visible white mat accumulation showed correlations with pH and other factors. Concentrations of THg within the non-white mat areas showed some correlation with multiple factors; however, not all of these were shared with the white mat areas, despite similarities in the ranges of concentrations of cations and anions. Smaller groupings showed potential similarities; however, these groupings were too small ($n < 4$) for meaningful statistical analysis. The highest THg concentrations from porewaters were found in samples associated with arc magmatic fluid, with sedimentation having a pivotal role in removing Hg (e.g., Crater site). Sediment samples showed elevated THg concentrations in the background and hydrothermally active areas, with active areas containing over double the background concentration. Duran-Toro et al. (2019) showed that suspended nanoparticles in the water column in Paleochori Bay were enriched in arsenic. Considering the Hg concentration difference between filtered and unfiltered samples, nanoparticles rich in Hg may exist in Paleochori Bay, which should be included in future research.

In summary, despite its substantial enrichment, we found Hg to be an elusive element in Paleochori Bay. Further investigations into the role of chemical reactions and fluid circulation in the shallow subsurface (before venting into seawater) will be necessary to better understand the source, transport and fate of Hg.

Declaration of Competing Interest

The authors declare that they have no known competing financial interests or personal relationships that could have influenced the work reported in this paper.

Acknowledgments

The authors would like to thank Athanasios Godelitsas, Anant Khimasia and Mike Vichos, who assisted in the field, to Henning Fröllje for laboratory support and to Carl Renshaw for discussions concerning the hydrothermal flux. This work was supported by the Deutsche Forschungsgemeinschaft (DFG) grant PI 746/10-1 to TP.

Appendix A. Supplementary data

Supplementary data to this article can be found online at https://doi.org/10.1016/j.marchem.2021.103984.

References

Aliani, S., Amici, L., Dando, P.R., Meloni, R., 1998. Time series of water pressure and bottom temperature in a marine shallow water hydrothermal vent of Milos Island (Aegean volcanic arc): preliminary results. Rapp. Comm. int. Mer Medit. 35, 46–47.
Andersson, M.E., et al., 2007. Seasonal and daily variation of mercury evasion at coastal and off shore sites from the Mediterranean Sea. Mar. Chem. 104 (3), 214–226.
Bagnato, E., et al., 2017. Hydrochemical mercury distribution and air-sea exchange over the submarine hydrothermal vents off-shore Panarea Island (Aeolian arc, Tyrrhenian Sea). Mar. Chem. 194, 63–78.
Barnes, H.L., 2015. Hydrothermal processes. Geochemical Perspectives 4 (1), 1–93.
Barnes, H., Seward, T., 1997. Geothermal systems and mercury deposits chapter 14. In: Geochemistry of hydrothermal ore deposits, 3rd ed. Wiley.
Barnes, H., Romberger, S., Stemprok, M., 1967. Ore solution chemistry;[part] 2, solubility of HgS in sulfide solutions. Econ. Geol. 62 (7), 957–982.
Bayraktarov, E., Price, R.E., Ferdelman, T.G., Finster, K., 2013. The pH and pCO(2) dependence of sulfate reduction in shallow-sea hydrothermal CO2 - venting sediments (Milos Island, Greece). Front. Microbiol. 4.
Berger, B.R., Eimon, P.I., 1983. Conceptual models of epithermal metal deposits in. In: Shanks, W.C. (Ed.), Cameron volume on unconventional mineral Depositss. Society of Mining Engineer, New York, pp. 191–205.
Bloom, N.S., Preus, E., Katon, J., Hiltner, M., 2003. Selective extractions to assess the biogeochemically relevant fractionation of inorganic mercury in sediments and soils. Anal. Chim. Acta 479 (2), 233–248.
Botz, R., et al., 1996. Hydrothermal gases offshore Milos Island, Greece. Chem. Geol. 130 (3–4), 161–173.
Bower, J., et al., 2008. Immobilization of mercury by pyrite (FeS2). Environ. Pollut. 156 (2), 504–514.

Bowman, K.L., Hammerschmidt, C.R., Lamborg, C.H., Swarr, G., 2015. Mercury in the North Atlantic Ocean: the U.S. GEOTRACES zonal and meridional sections. Deep-Sea Res. II Top. Stud. Oceanogr. 116, 251–261.
Bowman, K.L., Hammerschmidt, C.R., Lamborg, C.H., Swarr, G.J., Agather, A.M., 2016. Distribution of mercury species across a zonal section of the eastern tropical South Pacific Ocean (US GEOTRACES GP16). Mar. Chem. 186, 156–166.
Brombach, C.-C., Pichler, T., 2019. Determination of ultra-low volatile mercury concentrations in sulfur-rich gases and liquids. Talanta 199, 277–284.
Christenson, B., Mroczek, E., 2003. Potential reaction pathways of hg in some New Zealand hydrothermal environments. Special Publicat. Soc. Econ. Geol. 10, 111–132.
Cossa, D., Martin, J.-M., Takayanagi, K., Sanjuan, J., 1997. The distribution and cycling of mercury species in the western Mediterranean. Deep-Sea Res. II Top. Stud. Oceanogr. 44 (3), 721–740.
Cossa, D., et al., 2011. Mercury in the Southern Ocean. Geochim. Cosmochim. Acta 75 (14), 4037–4052.
Dando, P.R., et al., 1995. Gas venting rates from submarine hydrothermal areas around the island of Milos, Hellenic volcanic arc. Cont. Shelf Res. 15 (8), 913–929.
Davey, H.A., van Moort, J.C., 1986. Current mercury deposition at Ngawha Springs, New Zealand. Appl. Geochem. 1 (1), 75–93.
Dotsika, E., Poutoukis, D., Michelot, J.L., Raco, B., 2009. Natural tracers for identifying the origin of the thermal fluids emerging along the Aegean volcanic arc (Greece): evidence of arc-type magmatic water (ATMW) participation. J. Volcanol. Geotherm. Res. 179 (1), 19–32.
Duran-Toro, V.M., et al., 2019. Amorphous arsenic sulfide nanoparticles in a shallow water hydrothermal system. Mar. Chem. 211, 25–36.
Fitzgerald, W.F., Clarkson, T.W., 1991. Mercury and Monomethylmercury - present and future concerns. Environ. Health Perspect. 96, 159–166.
Fitzgerald, W.F., Lamborg, C.H., Hammerschmidt, C.R., 2007. Marine biogeochemical cycling of mercury. Chem. Rev. 107 (2), 641–662.
Fitzsimons, M.F., et al., 1997. Submarine hydrothermal brine seeps off Milos, Greece: observations and geochemistry. Mar. Chem. 57, 325–340.
Frederick, P., Jayasena, N., 2010. Altered pairing behaviour and reproductive success in white ibises exposed to environmentally relevant concentrations of methylmercury. Proc. R. Soc. B Biol. Sci. 278, 1851–1857.
Gamo, T., Glasby, G.P., 2003. Submarine hydorthermal activity in coastal zones. Land Marine Hydrogeol. 151–163.
Gworek, B., Bemowska-Kałabun, O., Kijeńska, M., Wrzosek-Jakubowska, J., 2016. Mercury in marine and oceanic waters—a review. Water Air Soil Pollut. 227 (10), 371.
Henley, R.W., 1995. In: Nicholson, K. (Ed.), Geothermal fluids: chemistry and exploration techniques. Springer Verlag, Berlin, New York, 1993, 263 pp., DM 138.00. Elsevier.
Horvat, M., et al., 1999. Mercury in contaminated coastal environments; a case study: the Gulf of Trieste. Sci. Total Environ. 237-238, 43–56.
Horvat, M., et al., 2003. Speciation of mercury in surface and deep-sea waters in the Mediterranean Sea. Atmos. Environ. 37, 93–108.
Hsu-Kim, H., Kucharzyk, K.H., Zhang, T., Deshusses, M.A., 2013. Mechanisms regulating mercury bioavailability for Methylating microorganisms in the aquatic environment: a critical review. Environ. Sci. Technol. 47 (6), 2441–2456.
Johnson, A., Cronan, D.S., 2001. Hydrothermal metalliferous sediments and waters off the Lesser Antilles. Marine Geosourc. Geotechnol. 19 (2), 65–83.
Khimasia, A., Renshaw, C., Price, R.E., Pichler, T., 2021. Hydrothermal flux and porewater geochemistry in Paleochori Bay, Milos, Greece. Chem. Geol. 571, 120188. Under Review.
King, J.K., Kostka, J.E., Frischer, M.E., Saunders, F.M., 2000. Sulfate-reducing bacteria methylate mercury at variable rates in pure culture and in marine sediments. Appl. Environ. Microbiol. 66 (6), 2430–2437.
Kuss, J., Holzmann, J., Ludwig, R., 2009. An elemental mercury diffusion coefficient for natural waters determined by molecular dynamics simulation. Environ. Sci. Technol. 43 (9), 3183–3186.
Lamborg, C.H., Fitzgerald, W.F., O'Donnell, J., Torgersen, T., 2002. A non-steady-state compartmental model of global-scale mercury biogeochemistry with interhemispheric atmospheric gradients. Geochim. Cosmochim. Acta 66 (7), 1105–1118.
Lamborg, C.H., Damm, K.L.V., Fitzgerald, W.F., Hammerschmidt, C.R., Zierenberg, R., 2006. Mercury and monomethylmercury in fluids from sea cliff submarine hydrothermal field, Gorda ridge. Geophys. Res. Lett. 33 (17).
Lamborg, C.H., et al., 2014. A global ocean inventory of anthropogenic mercury based on water column measurements. Nature 512 (7512), 65–68.
Leal-Acosta, M.L., Shumilin, E., Mirlean, N., Sapozhnikov, D., Gordeev, V., 2010. Arsenic and mercury contamination of sediments of geothermal springs, mangrove lagoon and the Santispac bight, Bahia Concepcion, Baja California peninsula. Bull. Environ. Contam. Toxicol. 85 (6), 609–613.
Lehnherr, I., St. Louis, V.L., Hintelmann, H., Kirk, J.L., 2011. Methylation of inorganic mercury in polar marine waters. Nat. Geosci. 4 (5), 298–302.
Liss, P.S., Slater, P.G., 1974. Flux of gases across the Air-Sea Interface. Nature 247 (5438), 181–184.
Mason, R., 2001. The Bioaccumulation of Mercury, Methylmercury and Other Toxic Elements into Pelagic and Benthic Organisms. Coastal and Estuarine Risk Assessment. CRC/Lewis Publ.
Mason, R.P., Sheu, G.R., 2002. Role of the ocean in the global mercury cycle. Glob. Biogeochem. Cycles 16 (4), 40-1-40-14.
McCarthy, K.T., Pichler, T., Price, R.E., 2005. Geochemistry of champagne Hot Springs shallow hydrothermal vent field and associated sediments, Dominica, Lesser Antilles. Chem. Geol. 224, 55–68.
Migdisov, A.A., Bychkov, A.Y., 1998. The behaviour of metals and Sulphur during the formation of hydrothermal mercury–antimony–arsenic mineralization, Uzon caldera, Kamchatka, Russia. J. Volcanol. Geotherm. Res. 84 (1), 153–171.
Miquel, J.C., Fowler, S.W., La Rosa, J., Aliani, S., Meloni, R., 1998. Particulate and organic fluxes in a coastal hydrothermal area off Milos. Aegean Sea. Rapp. Comm. int. Mer Medit. 35, 276–277.
Naden, J., Kilias, S.P., Darbyshire, D.P.F., 2005. Active geothermal systems with entrained seawater as modern analogs for transitional volcanic-hosted massive sulfide and continental magmato-hydrothermal mineralization: the example of Milos Island, Greece. Geology 33 (7), 541–544.
O'Hara, S.C.M., et al., 1994. Gas seep induced interstitial water circulation: observations and environmental implications. Cont. Shelf Res. 15 (8), 931–948.
Papachristou, M., Voudouris, K., Karakatsanis, S., D'Alessandro, W., Kyriakopoulos, K., 2014. Geological setting, geothermal conditions and hydrochemistry of south and southeastern Aegean geothermal systems. In: Geothermal Systems and Energy Resources. CRC Press Taylor & Francis Group, Turkey and Greece: London, pp. 47–75.
Pflumio, C., Boulegue, J., Liakopoulos, A., Briqueu, L., 1991. Oxygen, hydrogen, strontium isotopes and metals in the present-day and past geothermal systems of Milos Island (Aegean arc). In: Source, Transport and Deposition of Metals, pp. 107–112. Balkema, Rotterdam.
Pichler, T., Veizer, J., 2004. The precipitation of aragonite from shallow-water hydrothermal fluids in a coral reef, Tutum Bay, Ambitle Island, Papua New Guinea. Chem. Geol. 207 (1–2), 31–45.
Pichler, T., Giggenbach, W.F., McInnes, B.I.A., Buhl, D., Duck, B., 1999a. Fe-sulfide formation due to seawater-gas-sediment interaction in a shallow water hydrothermal system at Lihir Island, Papua New Guinea. Econ. Geol. 94, 281–288.
Pichler, T., Veizer, J., Hall, G.E.M., 1999b. The chemical composition of shallow-water hydrothermal fluids in Tutum Bay, Ambitle Island, Papua New Guinea and their effect on ambient seawater. Mar. Chem. 64 (3), 229–252.
Pichler, T., Veizer, J., Hall, G.E.M., 1999c. Natural input of arsenic into a coral-reef ecosystem by hydrothermal fluids and its removal by Fe(III) oxyhydroxides. Environ. Sci. Technol. 33 (9), 1373–1378.
Pichler, T., et al., 2019. Suitability of the shallow water hydrothermal system at Ambitle Island (Papua New Guinea) to study the effect of high pCO2 on coral reefs. Mar. Pollut. Bull. 138, 148–158.
Price, R.E., Giovannelli, D., 2017. A Review of the Geochemistry and Microbiology of Marine Shallow-Water Hyrothermal Vents (Reference Module in Earth Systems and Environmental Sciences).
Price, R.E., Pichler, T., 2005. Distribution, speciation and bioavailability of arsenic in a shallow-water submarine hydrothermal system, Tutum Bay, Ambitle Island, PNG. Chem. Geol. 224, 122–135.
Price, R.E., et al., 2013a. Processes influencing extreme as enrichment in shallow-sea hydrothermal fluids of Milos Island, Greece. Chem. Geol. 348, 15–26.
Price, R.E., et al., 2013b. Archaeal and bacterial diversity in an arsenic-rich shallow-sea hydrothermal system undergoing phase separation. Front. Microbiol. 4 (158), 1–19.
Prol-Ledesma, R.M., Canet, C., Torres-Vera, M.A., Forrest, M.J., Armienta, M.A., 2004. Vent fluid chemistry in Bahia Concepcion coastal submarine hydrothermal system, Baja California Sur, Mexico. J. Volcanol. Geotherm. Res. 137, 311–328.
Saunders, J.A., Brueseke, M.E., 2012. Volatility of se and Te during subduction-related distillation and the geochemistry of epithermal ores of the western United States. Econ. Geol. 107 (1), 165–172.
Saunders, J.A., et al., 2008. Genesis of middle Miocene Yellowstone hotspot-related bonanza epithermal au–ag deposits, northern Great Basin, USA. Mineral. Deposita 43 (7), 715–734.
Schroeder, W.H., Munthe, J., 1998. Atmospheric mercury–an overview. Atmos. Environ. 32 (5), 809–822.
Sievert, S.M., Brinkhoff, T., Muyzer, G., Ziebis, V., Kuever, J., 1999. Spatial heterogeneity of bacterial populations along an environmental gradient at a shallow submarine hydrothermal vent near Milos Island (Greece). Appl. Environ. Microbiol. 65 (9), 3834–3842.
Simmons, S.F., Brown, K.L., 2007. The flux of gold and related metals through a volcanic arc, Taupo volcanic zone, New Zealand. Geology 35 (12), 1099–1102.
Sonke, J.E., Heimbürger, L.-E., Dommergue, A., 2013. Mercury biogeochemistry: paradigm shifts, outstanding issues and research needs. Compt. Rendus Geosci. 345 (5–6), 213–224.
Stüben, D., Glasby, G.P., 1999. Geochemistry of shallow submarine hydrothermal fluids from Paleohori Bay, Milos, Aegean Sea. Explor. Min. Geol. 8 (3–4), 273–287.
Sun, R., et al., 2014. Mercury stable isotope signatures of world coal deposits and historical coal combustion emissions. Environ. Sci. Technol. 48 (13), 7660–7668.
Taran, Y.A., Hedenquist, J.W., Korzhinsky, M.A., Tkachenko, S.I., Shmulovich, K.I., 1995. Geochemistry of magmatic gases from Kudryavy volcano, Iturup, Kuril Islands. Geochim. Cosmochim. Acta 59 (9), 1749–1761.
UNEP, 2013. Global Mercury Assessment 2013 - Sources, Emissions, Releases and Environmental Transport.
USEPA, 2002. In: Water, O.O. (Ed.), Method 1631, revision E: mercury in water by oxidation, purge and trap, and cold vapor atomic fluorescence spectrometry.
Valsami-Jones, E., et al., 2005. The geochemistry of fluids from an active shallow submarine hydrothermal system: Milos island, Hellenic volcanic arc. J. Volcanol. Geotherm. Res. 148 (1–2), 130–151.
Voudouris, P., et al., 2021. Arsenian pyrite and cinnabar from active submarine nearshore vents, Paleochori Bay, Milos Island, Greece. Minerals 11 (1).
Wang, Y.M., et al., 2015. Elemental mercury in natural waters: occurrence and determination of particulate hg(0). Environ. Sci. Technol. 49 (16), 9742–9749.
Wängberg, I., et al., 2001. Estimates of air-sea exchange of mercury in the Baltic Sea. Atmos. Environ. 35 (32), 5477–5484.

Wanninkhof, R., 1992. Relationship between wind speed and gas exchange over the ocean. J. Geophys. Res. Oceans 97 (C5), 7373–7382.
Wenzhofer, F., Holby, O., Glud, R.N., Nielsen, H.K., Gundersen, J.K., 2000. In situ microsensor studies of a shallow water hydrothermal vent at Milos, Greece. Mar. Chem. 69, 43–54.
Wu, J., Wells, M.L., Rember, R., 2011. Dissolved iron anomaly in the deep tropical–subtropical Pacific: evidence for long-range transport of hydrothermal iron. Geochim. Cosmochim. Acta 75 (2), 460–468.
Yucel, M., et al., 2013. Eco-geochemical dynamics of a shallow-water hydrothermal vent system at Milos Island, Aegean Sea (eastern Mediterranean). Chem. Geol. 356, 11–20.